

Article

Performance Investigation and Cogging Torque Reduction in a Novel Modular Stator PM Flux Reversal Machine

Surat Khan ¹, Abdin Pasund ^{1,*} , Naseer Ahmad ^{1,2} , Shoaib Ahmed ¹ , Hamid Ali Khan ³ ,
Khalid Mehmood Cheema ⁴ and Ahmad H. Milyani ⁵ 

- ¹ Department of Electrical Engineering, Faculty of Information and Communication Technology, Balochistan University of Information Technology, Engineering and Management Sciences (BUIITEMS), Quetta 87300, Pakistan; surat.khan@buitms.edu.pk (S.K.); naseer.ahmad@uniroma1.it (N.A.); shoaib.ahmed@buitms.edu.pk (S.A.)
- ² Department of Electrical Engineering, Sapienza University of Rome, 00185 Rome, Italy
- ³ Department of Industrial Engineering, University of Trieste, 34127 Trieste, Italy; hamidalims@gmail.com
- ⁴ Department of Electronic Engineering, Fatima Jinnah Women University, Rawalpindi 46000, Pakistan; khalid.mehmood@fjwu.edu.pk
- ⁵ Department of Electrical and Computer Engineering, King Abdulaziz University, Jeddah 21589, Saudi Arabia; ahmilyani@kau.edu.sa
- * Correspondence: abdinpasund@gmail.com

Abstract: In this research paper, various performances of five different rotor pole topologies of the proposed novel modular stator (MS) permanent magnet (PM) flux reversal machine were investigated. The proposed design had concentrated, non-overlapping winding, which offered high average torque capability at a wide speed range. The no-load performances such as coil test analysis, three-phase flux linkage, flux distribution, back-EMF, and cogging torque, and load analysis, such as average torque versus current density, instantaneous torque, and average electromagnetic torque, were compared. The PM modular stator machine had high cogging torque, which created vibration and noise in the machine. Different cogging torque reduction techniques, such as notching, arc, flange and hybrid technique arc flange, arc notch, notch flange, and arc notch flange, were applied to reduce the cogging torque, improve average load torque, and reduce the induced voltage, harmonics, and torque ripples. The maximum cogging torque decreased by 87.66% and 82% when the arc notch flange and notch arc techniques were applied, respectively, and the minimum effect on cogging torque by the flange technique was 20.66%. Furthermore, the arc flange technique reduced the average torque by 66.72%. The maximum induced voltage was reduced by up to 12.83% using the notch arc technique. The hybrid technique of arc notch flange reduced the harmonics content in flux by 40% and enhanced electromagnetic performance. When applying the hybrid arc notch flange technique, torque ripples were reduced to 90.11%.

Keywords: flux reversal machine; modular stator; cogging torque; notching; hybrid techniques; finite element analysis



Citation: Khan, S.; Pasund, A.; Ahmad, N.; Ahmed, S.; Khan, H.A.; Cheema, K.M.; Milyani, H.A. Performance Investigation and Cogging Torque Reduction in a Novel Modular Stator PM Flux Reversal Machine. *Energies* **2022**, *15*, 2261. <https://doi.org/10.3390/en15062261>

Academic Editors: Nicu Bizon, Mihai Oproescu, Philippe Poure, Rocio Pérez de Prado and Abdessattar Abdelkefi

Received: 17 February 2022

Accepted: 14 March 2022

Published: 19 March 2022

Publisher's Note: MDPI stays neutral with regard to jurisdictional claims in published maps and institutional affiliations.



Copyright: © 2022 by the authors. Licensee MDPI, Basel, Switzerland. This article is an open access article distributed under the terms and conditions of the Creative Commons Attribution (CC BY) license (<https://creativecommons.org/licenses/by/4.0/>).

1. Introduction

PM machines have high efficiency, high torque density, and a robust structure; therefore, PM machines have attracted much attention in the last few decades [1,2]. A PM can be assigned to either the stator or rotor to excite the magnetic field. Due to their excellent cooling control and compact structure, PM machines with stator PMs have recently piqued the interest of researchers as all excitations are in the stator [3]. The idea of placing a PM in the stator was first used in a switched reluctance machine (SRM) to minimize magnetic saturation [4]. The magnetic field produced by a PM, on the other hand, is constant and thus difficult to control in traditional PM machines. As a result, hybrid excited machines that combine PM and dc winding have received a lot of attention [5]. Since slip rings and

brushes are needed for dc field excitation in the rotor, field coils in the stator are more acceptable for hybrid excited machines.

To combine the advantage of PM machines with high torque density and SRM with a compact rotor, flux reversal permanent magnet machines (FRPMMs) were developed in 1997 [6]. FRPMMs have the advantages of high fault tolerance, simple construction, high torque density, quick transient response, and easy maintenance [7]. As a result, FRPMMs are commonly used in a variety of applications, including electric drive propulsion [8], direct-drive wind power units [9], and low-speed servo motors [10]. FRPMMs have been designed and analyzed by several researchers with outstanding work [11]. An FRPMM has a higher power density than a standard fractional slot concentrated winding (FSCW) PM machine but a lower power factor. In terms of operation principle, inductance, torque capacities, and other factors, an FRPMM can be compared with other brushless machines such as the SRM, doubly salient PM machines, and brushless dc machines [12].

FRMs are classified into flux reversal permanent magnet machines (FRPMMs), field excited flux reversal machines (FEFRMs), hybrid permanent magnet flux reversal machines (HPMFRMs), and modular stator flux reversal permanent magnet machines (MSFRPMMs) [1]. The modular stator (MS) structure is a new method for machine melioration. The MS structure has the advantages of simplified manufacturing processes and high fault tolerance. In [4] a modular PM motor with a segmented stator was investigated, and it was found that if the flux gap and teeth width were appropriately chosen, the machine's efficiency could be dramatically increased. For safety-critical applications, a modular stator SRM was proposed in [13]. It demonstrated that the modular structure could improve reliability, making a fault-tolerant drive system possible. In [14] the authors presented two SRMs that used a c-core topology in a new way with a short magnetic flux in the stator, which provided higher performance in terms of power and winding design versatility, as well as maximum torque. However, few studies have been published on modular stator SRMs with PMs. To enhance the advantages of the MS technique, a novel MSFRPMM is proposed in this paper. An MSFRPMM has the advantages of stator slot PM machines, such as negligible cogging torque, high fault tolerance capacity, and less required volume for the PM.

In this paper, a novel modular stator PM flux reversal machine with non-overlapping winding is proposed. The proposed design was analyzed with five different rotor poles in terms of flux linkage, back-EMF, cogging torque, and load torque. An eight-pole modular stator machine was selected for applying the cogging torque reduction technique because it has the highest cogging torque. The operation principle of the machine is presented in Section 2. The design methodology and geometric values are presented in Section 3. The rotor pole study is investigated in Section 4. Finally, finite element analysis (FEA) on no-load, load analysis, electromagnetic performances comparison, and cogging torque reduction techniques are presented in Section 5. The conclusion of the research is discussed in Section 6.

2. Operation Principle

Flux reversal machines operate on the principle of flux reversal in the rotor pole in front of one stator slot movement. This change of flux causes the creation of bipolar sinusoidal back-EMF. The bipolar flux and the sinusoidal back-EMF causes the induction of torque in the rotor. Different rotor poles and stator winding layouts are analyzed in this paper to select a higher load torque machine.

2.1. Rotor Poles and Stator Slots

To obtain a sinusoidal no-load back-EMF with low harmonic distortion, appropriate combinations of rotor poles and stator slots were selected. Due to modulation of the rotor permeance even order harmonics and back-EMF of the MSFRM suffered from even order harmonics. To achieve a sinusoidal back-EMF, coils with even opposite order back-EMF were connected in one phase. As shown in Figure 1a and vector diagram Figure 1b, a

null harmonic distribution factor was obtained when the phase number m and stator slots number N_s satisfied the following:

$$N_s = 2 km \tag{1}$$

where, $k = 1, 2, 3, \dots$

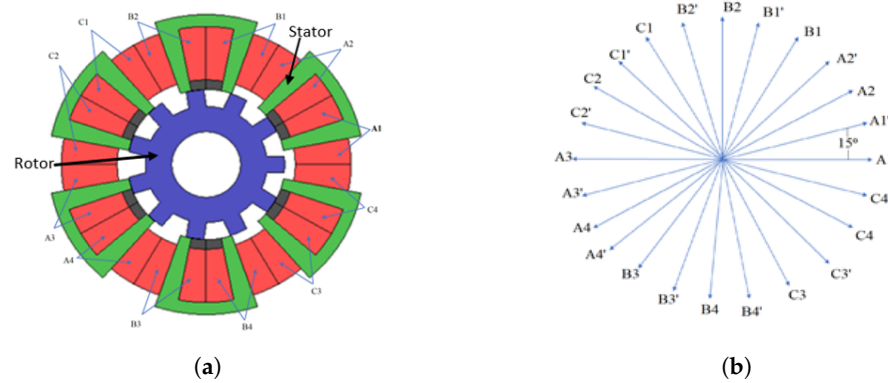


Figure 1. Coil-phase arrangement of the proposed model. (a) Phase-coil connections. (b) Phase-coil connection vectors.

2.2. Winding Layout

A PMFRM consists of U-shaped laminated segments, NEOMAX-35AH, with circumferential anisotropic pattern magnets, windings, and a salient rotor. A PMFRM has concentrated winding, including single layer, double layer, and multilayer windings. A single layer winding stator slot N_s and rotor pole N_r must satisfy the following equation:

$$\frac{LCM(N_s, N_r)}{N_r} = 12k \tag{2}$$

A double layer winding must satisfy the equation

$$\frac{LCM(N_s, N_r)}{N_r} = 6k \tag{3}$$

Here, LCM stands for the least common multiple of its arguments and k is an integer. The angular slot pitch for concentrated winding is computed as follows:

$$\theta_s = 360^\circ E \frac{N_r}{N_s} \tag{4}$$

Here, E indicates electrical degree.

The relative angle of all potential coils having a slot of i is as follows:

$$\theta_c(i) = (i - 1)\theta_s \tag{5}$$

For $i = 1, 2, 3, \dots, N_s$

In three phases, windings were separated by $120^\circ E$ from other phases. The offset of K° slots is an integer value computed by the following:

$$K = \frac{N_s}{3N_r} (1 + 3q) \tag{6}$$

Here $q = 1, 2, 3, \dots, (N_r - 1)$

3. Design Methodology

The Japan Research Institute launched the JMAG Designer 14.1 version for solving 2D-FEA in machine design. To draw stator, rotor, armature coil, and permanent magnet

geometry an editor is used. JMAG Designer can also be used to assign the design machine's material conditions, circuits, and properties. A NEOMAX-35AH with circumferential Anisotropic Pattern was used for the permanent magnets, 35H210 steel was used for the rotor and stator, and copper was used for armature coils in the JMAG designer. Parameters of the model are given in Figure 2 and Table 1. This paper aimed to design high average torque, low cogging torque, high fault tolerance, low cost, and a robust rotor structure modular stator flux reversal permanent magnet machine. The following steps were executed for the design procedure.

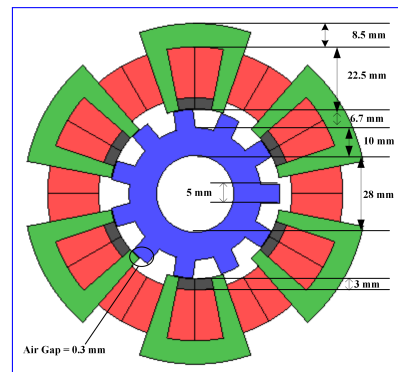


Figure 2. Parameters of the model.

Table 1. Design parameters of the proposed modular rotor PMFRM.

Parameters	Value
Number of phases	3
Armature current density J_a	30
Number of stator slots	12
Rotor pole	8, 10, 11, 13, 14
Outer radius of stator (mm)	62
Stack length (mm)	60
Air gap b/w stator rotor (mm)	0.3
Armature slot area (mm ²)	157.16
No. of turns per armature coil slot	80

4. Rotor Pole Study and Flux Distribution

Almost all topologies have many restrictions; magnetic flux leakage at the tips of a PM is the main limitation. Consequently, flux distribution between segments is limited. To limit the above restriction, the following equations were applied for the calculation of rotor poles, and Figure 3 illustrates various rotor poles.

$$N_r = N_s \left(1 + \frac{k}{2q}\right) \quad (7)$$

Here, q = number of phases.

The maximum value of armature current density can be determined by the following equation:

$$J_a = \frac{I_a N_a}{\alpha_a S_a} \quad (8)$$

Here

J_a = current density,

N_a = number of turns,

α_a = filling factor,

S_a = slots area,

I_a = input current,

Subscript a represents an armature coil.

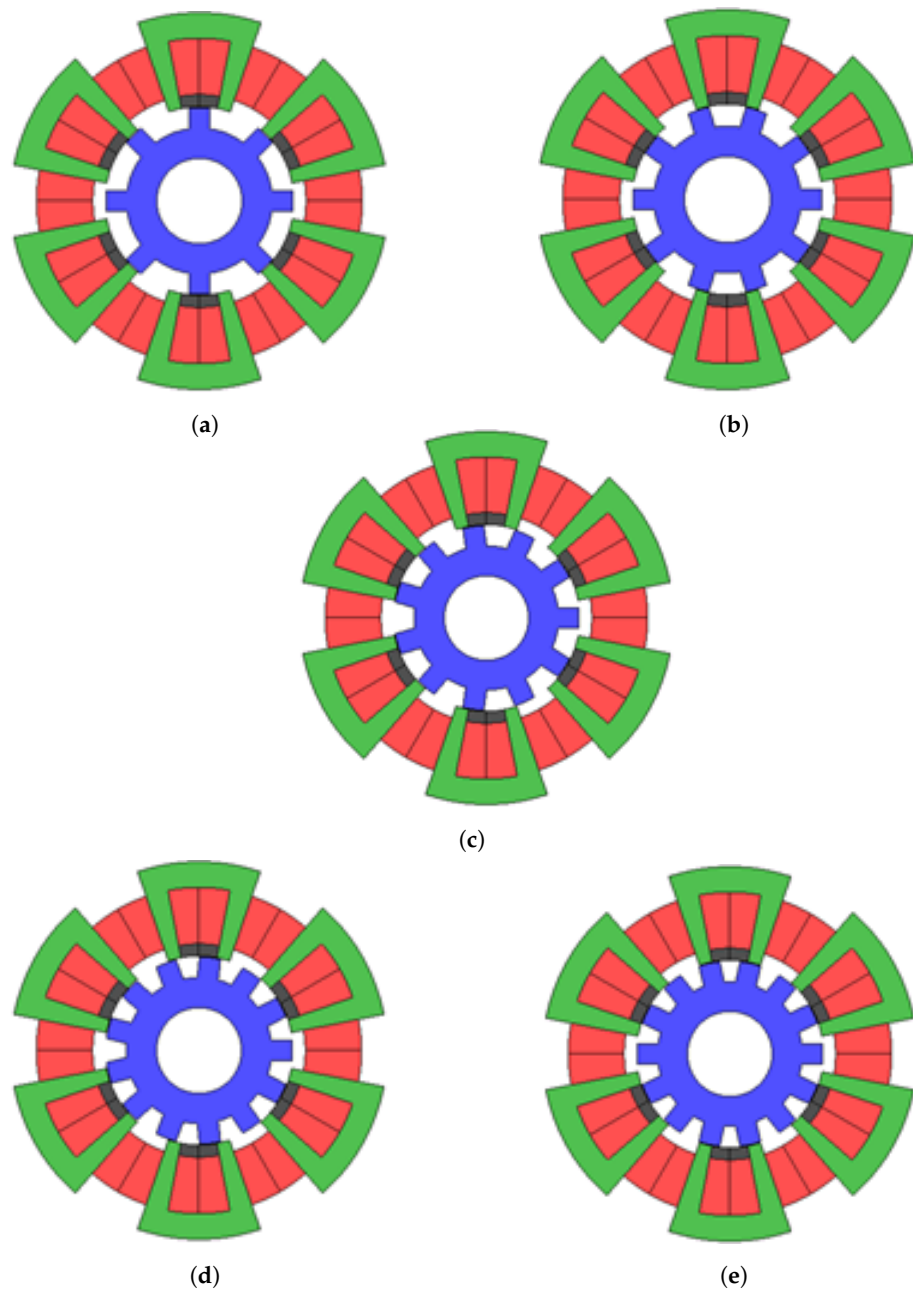


Figure 3. Various rotor poles of a modular stator PM flux reversal machine. (a) 8-P/12-S. (b) 10-P/12-S. (c) 11-P/12-S. (d) 13-P/12-S. (e) 14-P/12-S.

Figure 4 depicts the flux distributions at various rotor locations. Only the rotor PMs excited the magnetic field, and each rotor movement was 90 electrical degrees apart. Considering phase “A” flux linkage, when the rotor position was zero electrical degrees, the flux linkages were at their negative maximum, as shown in Figure 4a; when the rotor position was 90 electrical degrees, the flux linkage was zero, as shown in Figure 4b; when the rotor position was 180 electrical degrees, the flux linkage was at its positive maximum as shown in Figure 4c; and when the rotor position was 270 electrical degrees, the flux linkage was zero, as shown in Figure 4d. As a result, the flux reversed the polarity in 360 electrical degrees (one rotor slot pitch); therefore, it was called a “flux reversal machine”.

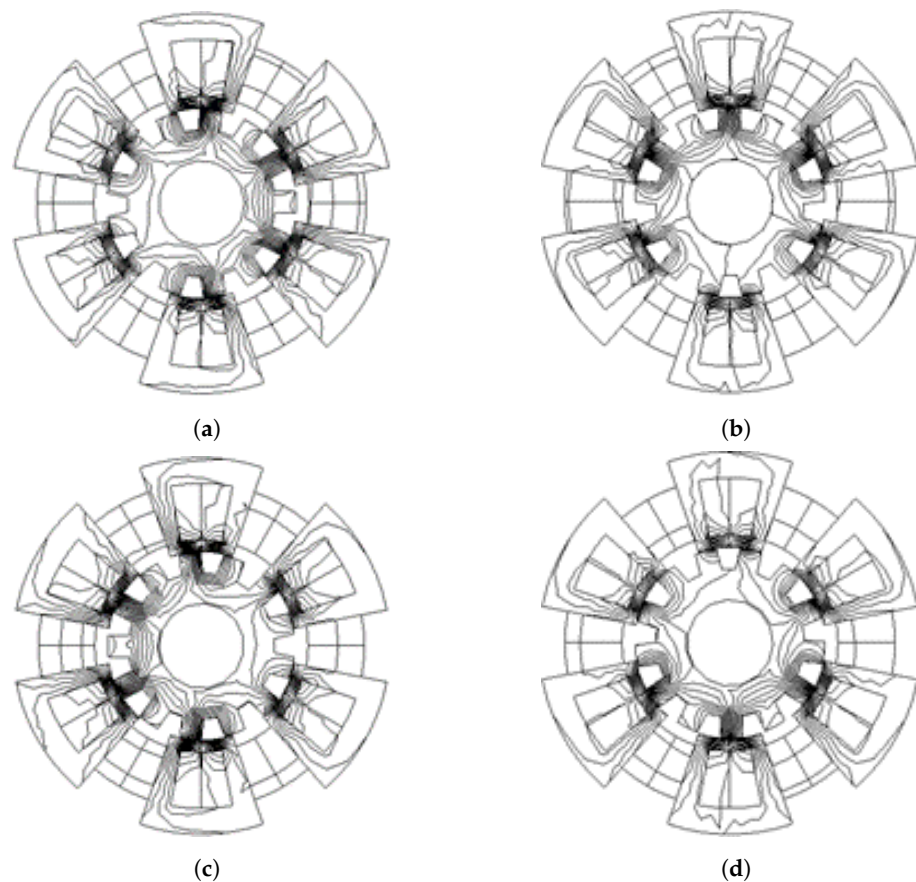


Figure 4. Flux distribution at various electrical degrees. (a) 0° . (b) 90° . (c) 180° . (d) 270° .

5. Results and Discussion

5.1. Coil Arrangement Test

The performance of the MSFRPMM was verified by a coil arrangement test, and flux linkage was investigated in each coil. PM is used to generate field flux. The performance of the coil was tested on no-load and magnetic flux linkage was observed. Three-phase flux linkage is shown in Figure 5, and odd and even rotor pole armature coil combinations are illustrated in Figure 6a,b, respectively. Different coil combinations were used in odd and even rotor pole topologies to generate bipolar armature flux linkage.

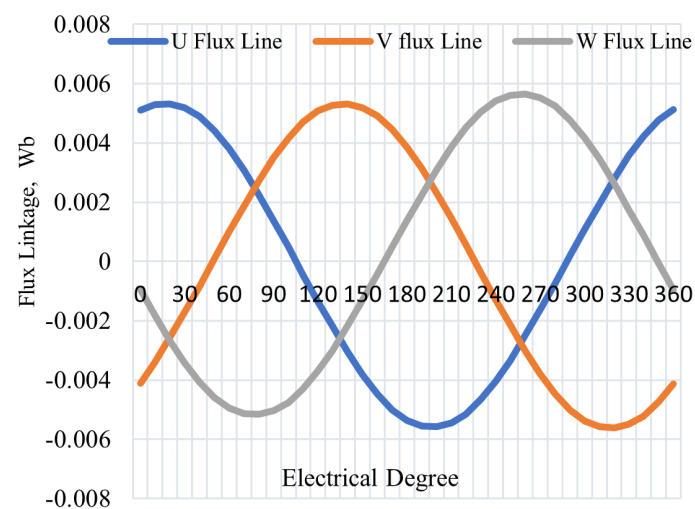


Figure 5. Three-phase flux linkage.

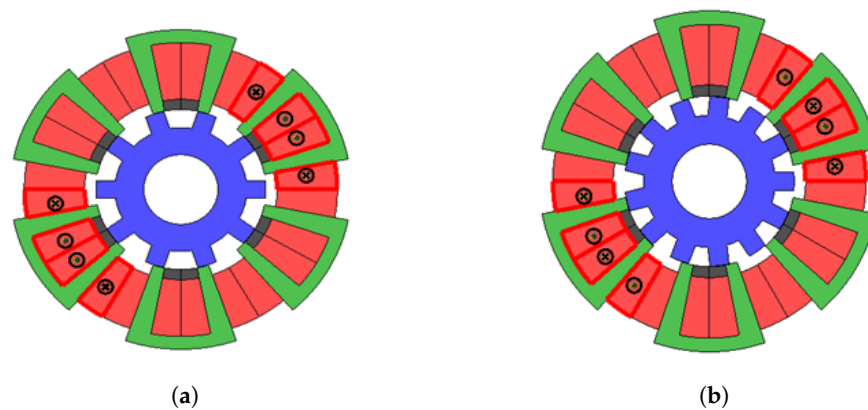


Figure 6. Armature coil “A” configuration. (a) 10-rotor pole. (b) 13-rotor pole.

5.2. U-Phase Flux Linkage

The operation principle of the MSFRPMM was verified by investigating the magnetic flux linkage in all three armature coils. The flux linkage was observed on no-load as shown in Figure 7. In this paper, flux linkage for different rotor poles under constant PM field flux at 400 rpm motor speed was observed. In Figure 7, five different rotor poles with 12 stator slots MSFRPMM are illustrated. In Figure 7, 13-pole and 11-pole machines had maximum amplitude flux linkages of 0.00676 Wb and 0.0086 Wb, respectively. Our results determined that 13- and 11-pole topologies were best due to the uniform magnetic force in their rotors.

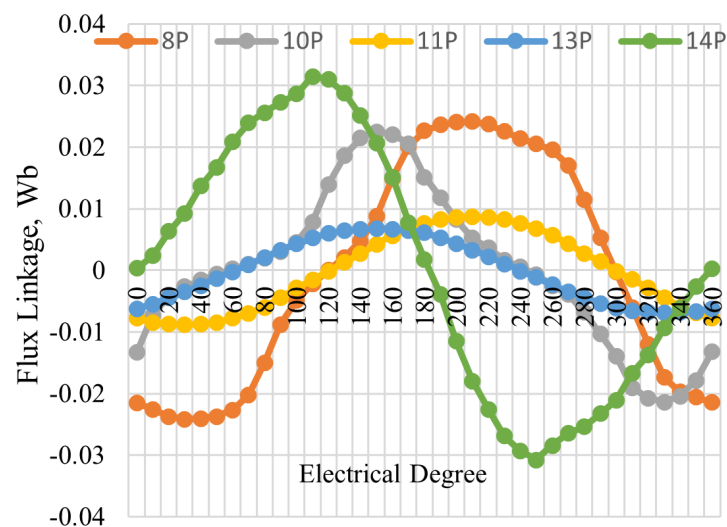


Figure 7. No-load flux of different rotor poles.

5.3. Cogging Torque

Figure 8 shows the cogging torque of all proposed machines. The topologies with 10, 14, and 8 rotor poles had the highest cogging torques, respectively, and the topologies with 13 and 11 rotor poles had the minimum cogging torque, as shown in Figure 8. Different techniques such as skewing notching could reduce the cogging torque, which could be improved by changing the machine structure. Aside from torque density, pulsating torque was also critical since a high pulsating torque increases machine noise and vibration. The ripple and cogging torque waveforms of the 8, 10, 11, 13, and 14 rotor poles of the MSFRPMM are shown in Figure 8. All these machines had a 12-stator slot number. It was shown that the 8 rotor poles of the MSFRPMM had the highest-rated cogging torque amplitude among the five machines. When it came to cogging, pulsating and ripple torque of the 8 and 10 rotor slots of the MSFRPMM were the highest, whereas the ripple and cogging torque of the 11 and 13 rotor slots of the MSFRPMM were the lowest. The least

common multiple of the rotor and stator slot numbers was linked to this phenomenon. The lowest was the pulsating torque, the greater was the least common multiple. As a result, the MSFRPMM with 11 rotor slots had the minimum ripple and cogging torque. However, care should be taken when using an odd rotor number, as this could result in other issues, such as eccentricity stress.

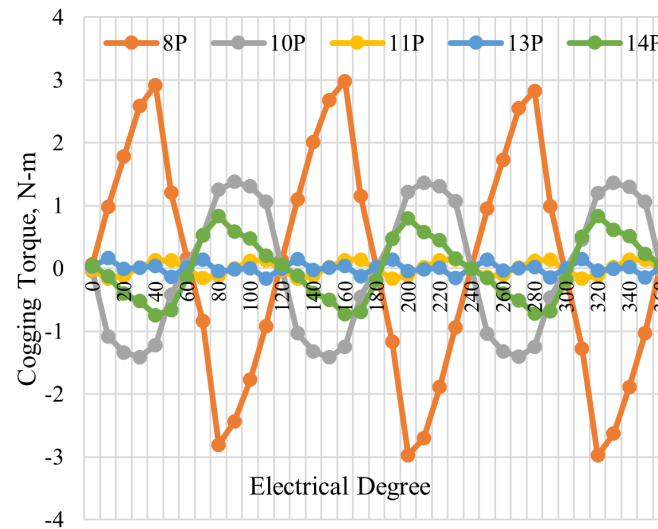


Figure 8. Cogging torque of different rotors.

5.4. Back-EMF

The no-load, back-EMF waveforms were nearly identical, as can be seen in Figure 9. The back-EMF waveforms of these five motors were sinusoidal because the coils' positive and negative magnetic flux paths were perfectly symmetrical and opposite, resulting in a sinusoidal coil back-EMF. The highest back-EMF and lowest back-EMF were 14-pole and 13-pole, respectively.

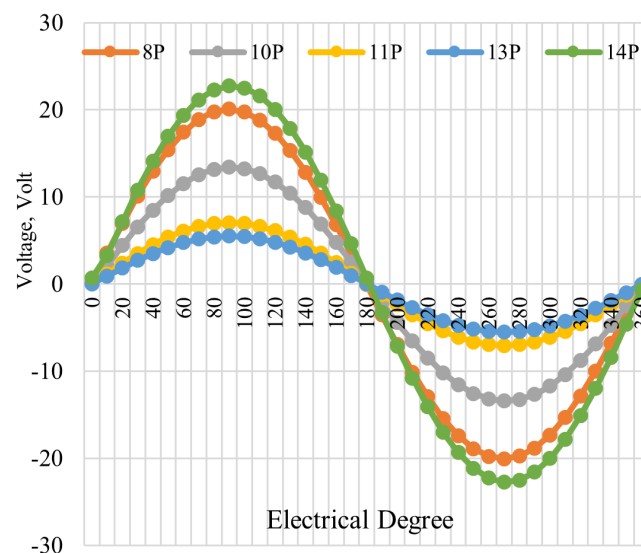


Figure 9. No-load back-EMF of different rotors.

5.5. Instantaneous Torque

Figure 10 shows the instantaneous electromagnetic torque for various rotor poles at a load current of 30 Arms . This showed the instantaneous torque of different proposed topologies. Instantaneous torque is the torque of full load at maximum armature current

30Arms. The instantaneous torque amplitudes of 10 rotor poles and 14 rotor poles were 18.85 N-m and 15.65 N-m, respectively, which were the highest in amplitude with the most considerable ripples. In comparison, topologies of the 13 rotor poles and 11 rotor poles had instantaneous torque amplitudes of 5.478 N-m and 5.98 N-m, respectively, with almost constant amplitude. Therefore, topologies with 13-rotor-pole and 11-rotor-pole combinations were the best topology in this regard.

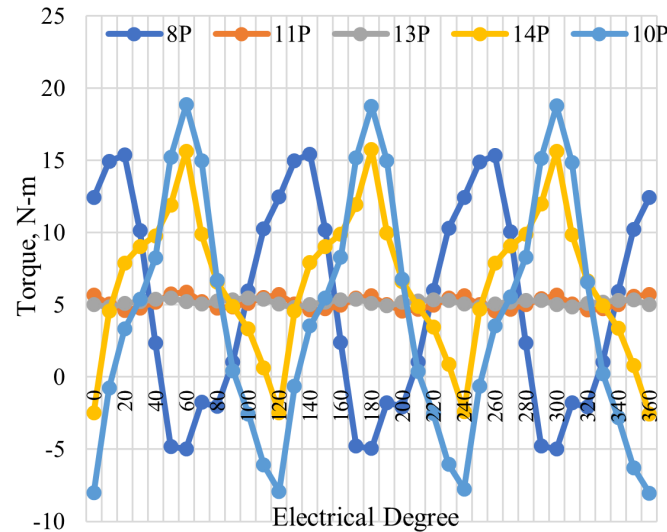


Figure 10. Instantaneous torques of different rotors.

5.6. Average Torque vs. Current Density

Figure 11 shows the instantaneous torque of different proposed topologies. Instantaneous torque is the torque of a full load at maximum armature current 30Arms. This showed that the instantaneous torque amplitudes of 10 rotor poles and 14 rotor poles were 4.65 N-m and 6.85 N-m, respectively, and they were the highest in amplitude with the largest ripples while topologies of 13 rotor poles and 11 rotor poles had instantaneous torque amplitudes of 5.18 N-m and 5.124 N-m, respectively, with almost constant amplitude.

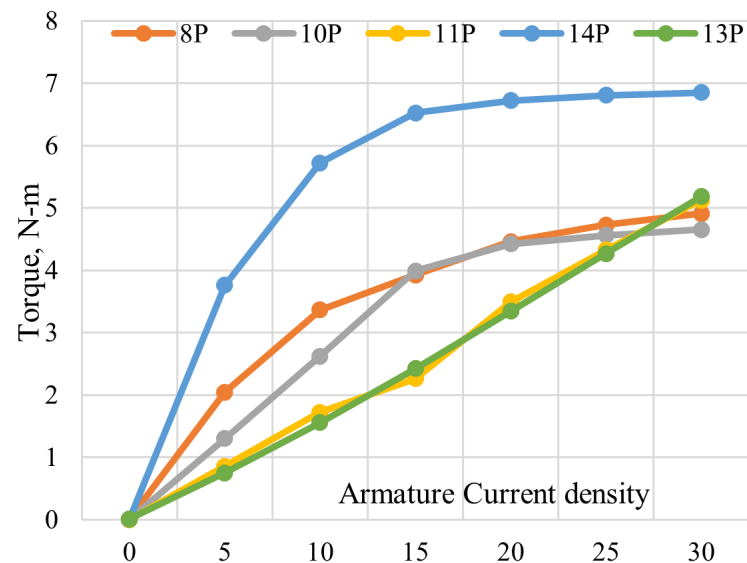


Figure 11. Average torques of different rotors.

Furthermore, machines with 8, 10, and 14 rotor poles had slightly more significant instantaneous torque ripples than motors with 11 and 13 rotor poles. The pulsating torque in 8, 10, and 14-rotor-pole motors were third-order harmonics, while 11 and 13-rotor-pole motors had the lowest pulsating torque with sixth-order harmonics. The instantaneous electromagnetic torque with a pure sine wave current drive was derived in Equation (9); when $I_d = 0$, control was used, and magnetic saturation on load was ignored to explain the pulsating torque component.

$$T_e = \frac{e_a i_a + e_b i_b + e_c i_c}{\omega_r} + T_c = \frac{3I_m E_1}{2\omega_r} + \frac{3I_m E_{3k-1} \cos 3k\omega_e t}{2\omega_r} + \frac{3I_m E_{3k+1} \cos 3k\omega_e t}{2\omega_r} + T_c \quad (9)$$

The third pulsating torque was generated because there were sizeable second-order harmonics in the back-EMF in the 8, 10, and 14 rotor poles. The third-order pulsating torque harmed the output torque efficiency with a high amplitude and low order. As a result, the 11- and 13-rotor-pole motors outperformed the 8, 10, and 14-rotor-pole motors in terms of torque ripple and average torque.

5.7. Selection of Design for Cogging Torque Reduction

Cogging torque was critical since a high pulsating cogging increases machine noise and vibration [15]. The ripple and cogging torque waveforms of the 8, 10, 11, 13, and 14 rotor poles of the modular stator permanent magnet flux reversal machine are shown in Figure 8. All these machines had a 12-stator slot number. The 8 rotor poles of the modular stator permanent magnet flux reversal machine had the highest-rated cogging torque amplitude among the five machines. When it came to cogging, the pulsating and ripple torque of the 8 and 10 rotor slots of the modular stator permanent magnet flux reversal machine were the highest. The highest cogging torque of the 8-rotor-pole machine needed to be reduced to a safe limit. This paper dealt with a different method for reducing the cogging torque of the 8-rotor-pole modular stator permanent magnet flux reversal machine to a safe limit.

Figure 12 shows the cogging torque of the given modular stator flux reversal machine with 8 poles. Cogging torque is the torque produced due to the change of reluctance of the flux path of the permanent magnets [16,17]. Cogging torque was at its maximum when the rotor pole came to the face of a permanent magnet, and it was at its minimum when the rotor pole was at the largest distance from the permanent magnets [18,19]. High cogging torque produces vibration, noise, and increases the losses of the machine [20,21]. Therefore, cogging torque needs to be minimized. The cogging torque of the selected modular stator permanent magnet flux reversal machine was very high. Its value was 6 N-m peak to peak. In this paper, different techniques of cogging torque reduction were applied to reduce the unwanted cogging torque. The dimensions of unoptimized model are shown in Figure 13.

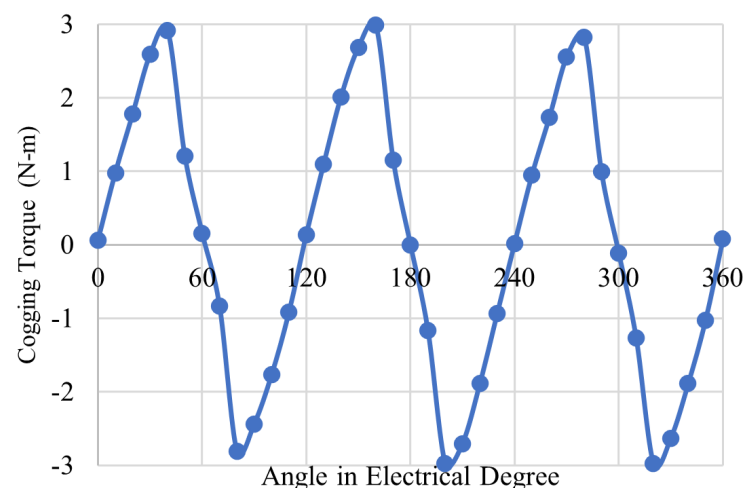


Figure 12. Average torque of different rotors.

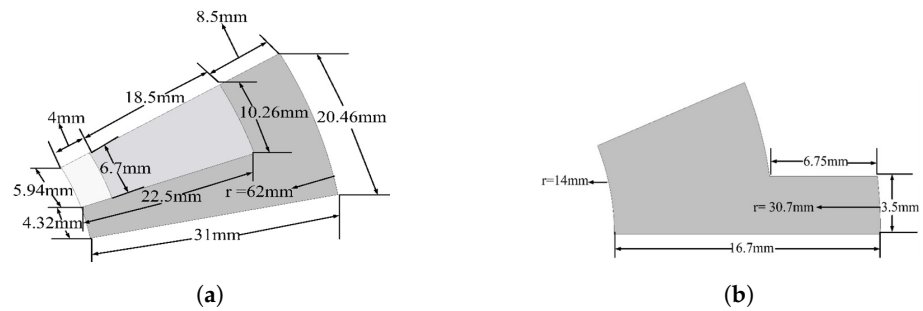


Figure 13. Parameters to be optimized. (a) Stator. (b) Rotor.

5.7.1. Notching

Applying a groove in the rotor pole tip is called notching, as shown in Figure 14. Notching creates a change in the reluctance of the flux path. To achieve the best results, a deterministic optimization technique of notching is applied. Each notch was different in width and depth from the other notches. The best result of the notching reduced the cogging torque from 6 N-m to 4.46 N-m peak to peak, a decrease of 25.66%, at a notch width of 1.05 mm and depth of 1 mm, as shown in Figure 14. A different result achieved by notching is shown in Figure 15.

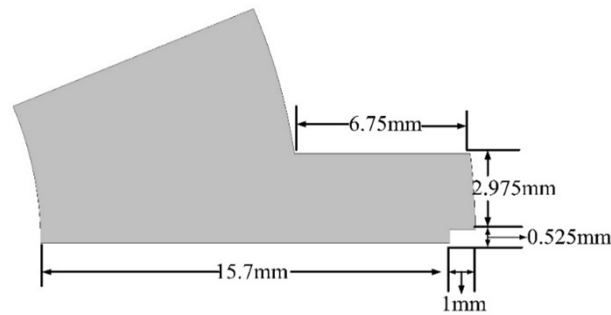


Figure 14. Notching in the rotor pole.

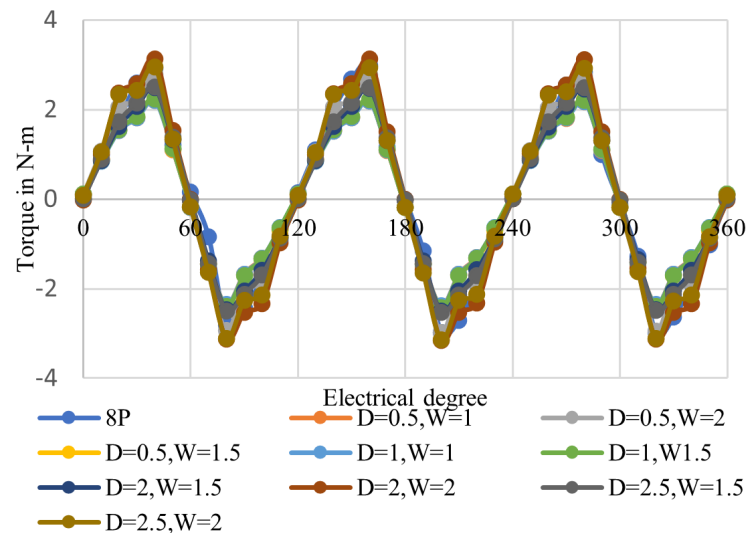


Figure 15. Different notching results.

5.7.2. Arc of the Rotor Pole

Figure 16 shows the arc in the rotor pole. Arc in the rotor pole caused a different reluctance in the flux path at the tip of the rotor pole with respect to the lower limb of the rotor pole. The change of reluctance due to the arc in the rotor pole caused a reduction in the cogging torque. Different results obtained by changing the arc are given in Figure 17.

A reduction of 29.66% in the cogging torque at the minimum 4.22 N-m peak to peak was achieved by an arc of 14.7°.

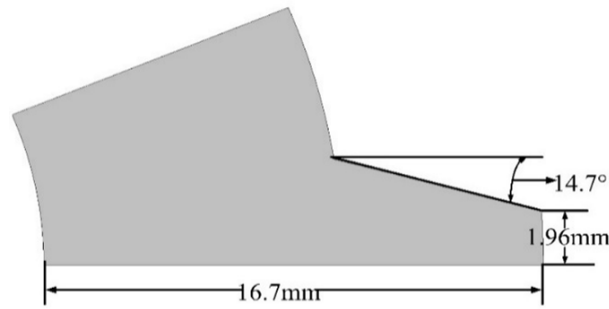


Figure 16. Arcing of the rotor pole.

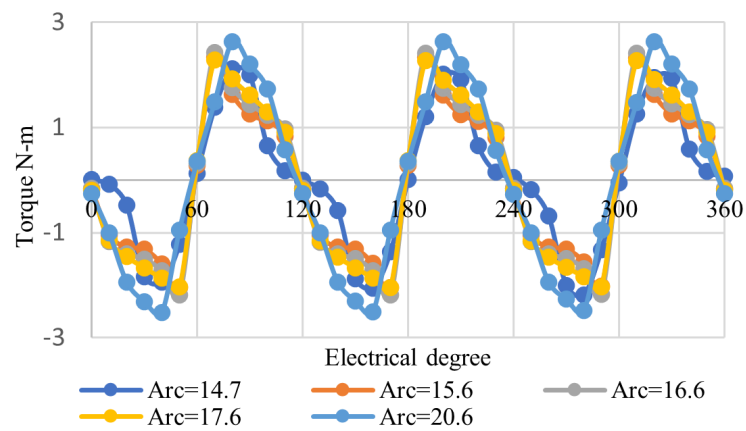


Figure 17. Different arcing result.

5.7.3. Flange of the Rotor Pole

Increasing the pole tip surface area is called flanging of the rotor pole, as shown in Figure 18. Flanging the rotor pole provided more surface area in front of the permanent magnets, decreasing the reluctance of the flux path for more electrical angles. The reduction in reluctance due to flanging caused a reduction in cogging torque. The best result of flanging caused a reduction in the cogging torque of 20.66%. The minimum cogging torque 4.76 N-m was achieved by a flange of 2 mm. Different flange results are shown in Figure 19.

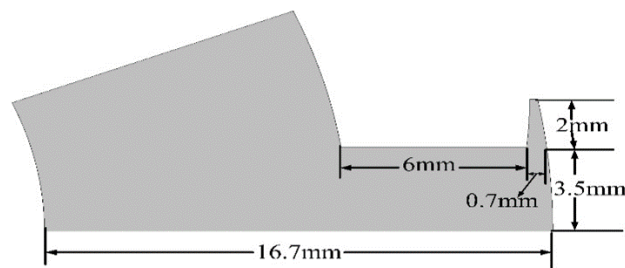


Figure 18. Flange of the rotor pole.

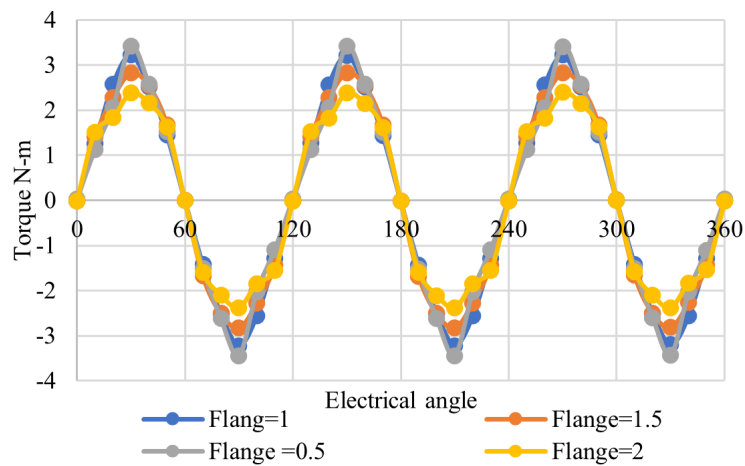


Figure 19. Different flanging results.

5.7.4. Hybrid Notch and Flange

Figure 20 shows the hybrid of a notch and flange. Notching increases the reluctance of flux path, while flanging provides extra length and reduces the reluctance. The hybrid combination of a notch with a depth of 2 mm and width of 2 mm and flange of 2 mm caused the overall cogging torque to increase to 6.64 N-m, an increase of 10.66%. The results of different hybrid notches and flanges are shown in Figure 21.

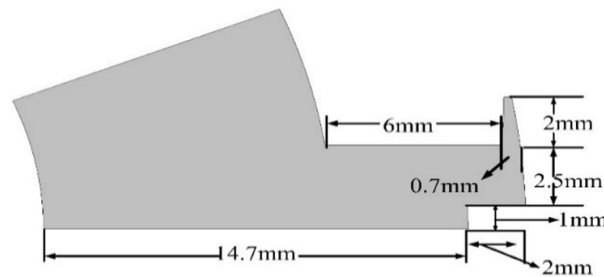


Figure 20. Hybrid (notch and flange) of the rotor pole.

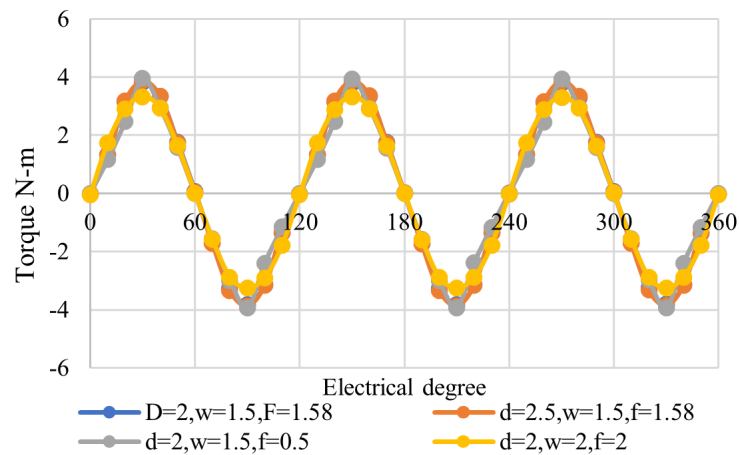


Figure 21. Results of hybrid (notch and flange).

5.7.5. Hybrid Notch and Arc

Figure 22 shows the hybrid technique of a notch and an arc. Due to the notch and arc in the rotor pole tip the reluctance of the flux path increased. Therefore, the overall cogging torque of the machine decreased to a large value. A notch with a width of 2 mm, a depth of 2 mm, and an arc of 11° caused a cogging torque reduction of 82%, which was 1.08 N-m

peak to peak. Different results using the hybrid notch and arc technique are shown in Figure 23.

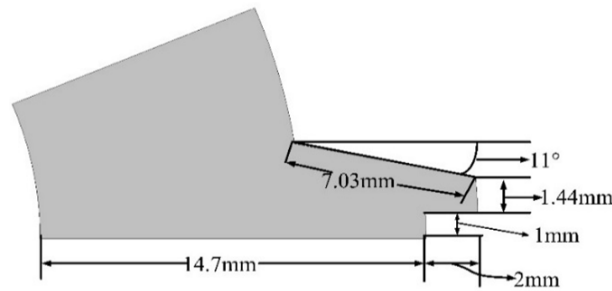


Figure 22. Hybrid (notch and arc) of the rotor pole.

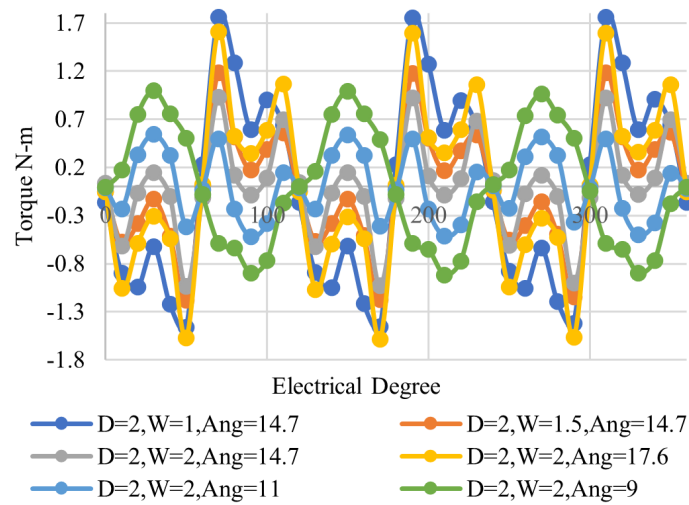


Figure 23. Results of hybrid (notch and arc).

5.7.6. Hybrid Arc and Flange

Figure 24 shows the hybrid technique of arc and flange. Arc in the rotor pole decreased the pole tip and increased the reluctance of the flux path, resulting in a decrease in cogging torque. At the same time, flange in the smaller rotor pole tip caused a slight increase in reluctance and, therefore, a small increase in cogging torque. The hybrid technique of arc and flange resulted in an overall decrease in cogging torque. The lower resultant cogging torque of 1.16 N-m, a reduction of 80.66%, was achieved by an arc of 20.6° and a flange of 1.55 mm. Results of different hybrid arc and flange are shown in Figure 25.

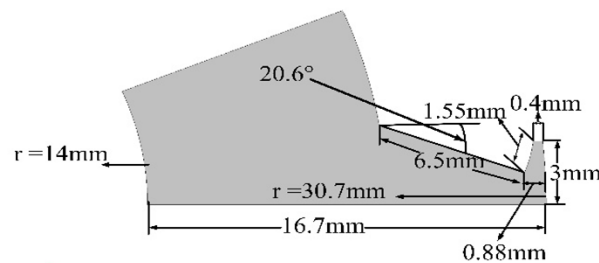


Figure 24. Hybrid (arc and flange) of the rotor pole.

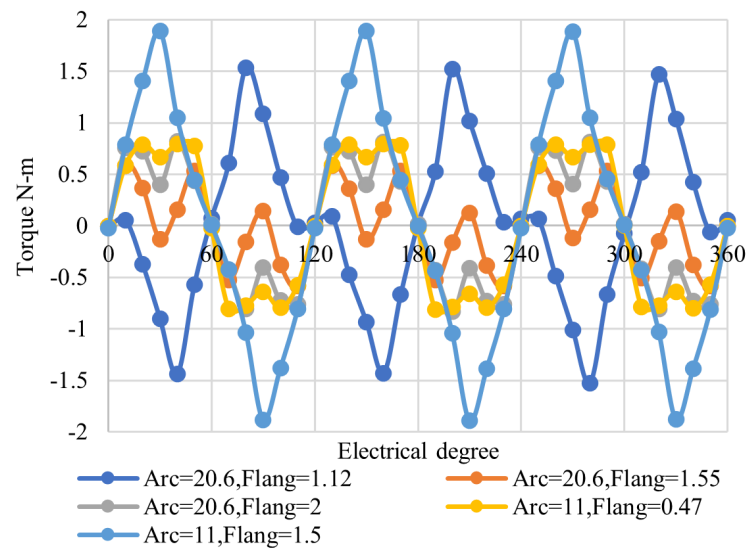


Figure 25. Results of hybrid (arc and flange).

5.7.7. Hybrid Arc, Flange, and Notch

A diagram of the hybrid arc, flange, and notch technique is given in Figure 26. The reluctance of the flux path was increased due to the arc, notch, and flange. Therefore, the resultant cogging torque decreased significantly due to arc and notch, and a small flange on the minimum rotor pole tip increased the reluctance. An overall cogging torque reduction of 87.66%, 0.74 N-m, was achieved by an arc of 14.7° , a flange of 0.43 mm, and a notch with a the depth of 1.5 mm and a width of 1.5 mm. Different results for the arc, flange, and notch are shown in Figure 27.

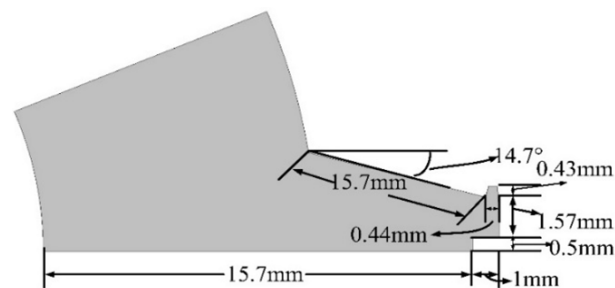


Figure 26. Hybrid (arc, flange and notch) of the rotor pole.

5.8. Effect of Cogging Torque Reduction Techniques on No-Load Flux

By applying the single variable optimization technique of arc, no-load flux was decreased by 11%; due to the flange technique no-load flux increased by up to 10.39%; no-load flux decreased by 5.28% when applying the notching technique; a decrease in no-load flux of 12% was observed by applying the hybrid arc and flange technique; the hybrid notch and arc technique caused a decrease of 28% in no-load flux; the hybrid notch and flange technique caused an increase of 10.95% in no-load flux; and the hybrid arc, notch, and flange technique caused an increase of 17.47% in no-load flux, as shown in Figure 28.

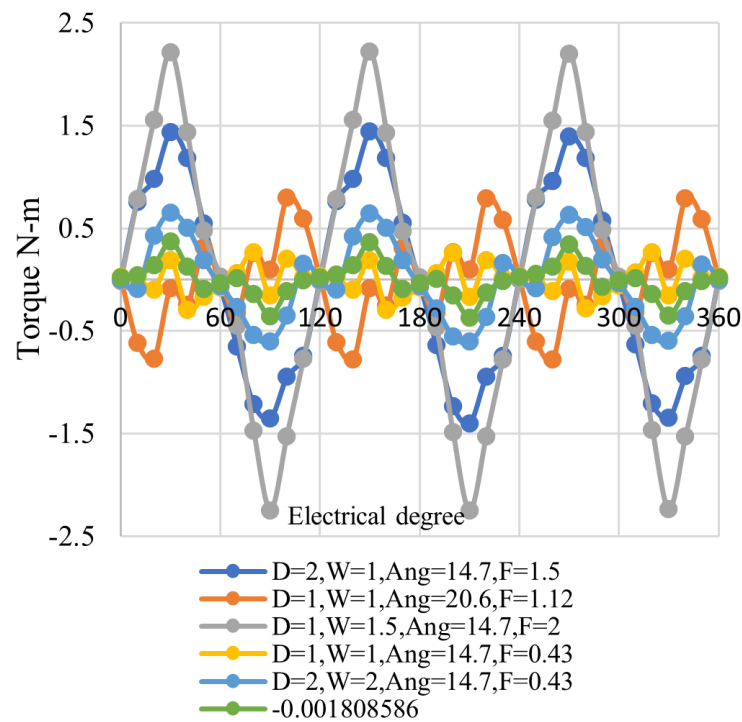


Figure 27. Results of hybrid (arc, flange, and notch).

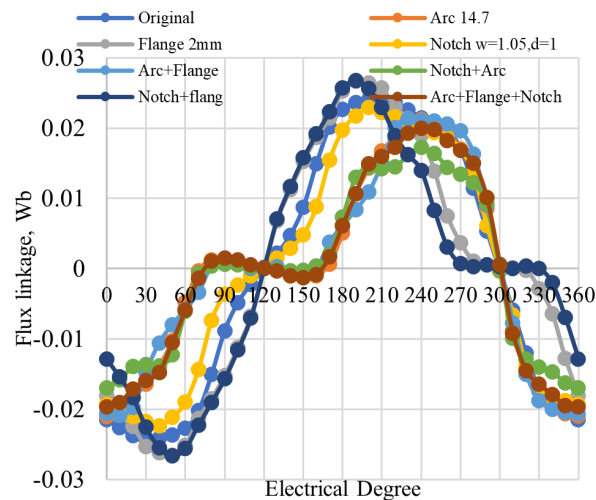


Figure 28. Flux linkage of all models.

5.9. Effect of Cogging Torque Reduction Techniques on No-Load Back-EMF

The no-load back-EMF waveforms were nearly identical, as can be seen in Figure 29. The back-EMF waveforms of these eight motors were sinusoidal because the positive and negative magnetic flux paths of the coils were perfectly symmetrical and opposite, resulting in a sinusoidal coil back-EMF.

By applying the deterministic optimization technique of arc, no-load back-EMF was decreased by 0.846%; due to the flange technique back-EMF increased by up to 49.717%; a 39.25% increase in back-EMF was observed when applying the notching technique; no change in back-EMF occurred when applying the hybrid arc and flange technique; the hybrid notch and arc technique caused a decrease of 12.83%; the hybrid notch and flange technique caused an increase of 33.05% in back-EMF; and the hybrid arc, notch, and flange technique caused an increase of 2.83% in back-EMF, as shown in Figure 29.

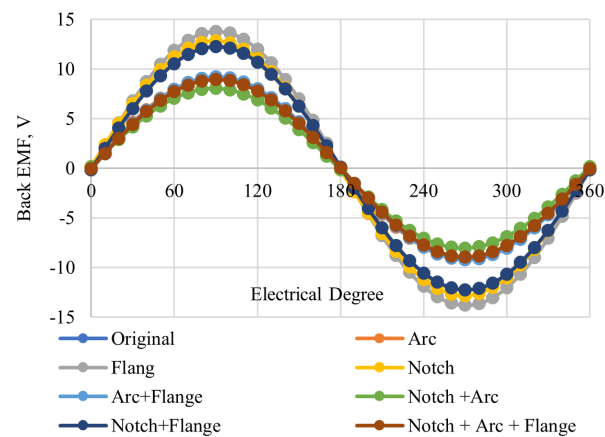


Figure 29. The no-load back-EMF of all models.

5.10. Effect of Cogging Torque Reduction Techniques on Harmonics

The magnetic field harmonics of the different designs are shown in Figure 30. It can be observed that applying the hybrid technique of notch, arc, and flange improved the working harmonic contents owing to superposition occurring in flux modulation that enhanced electromagnetic performance.

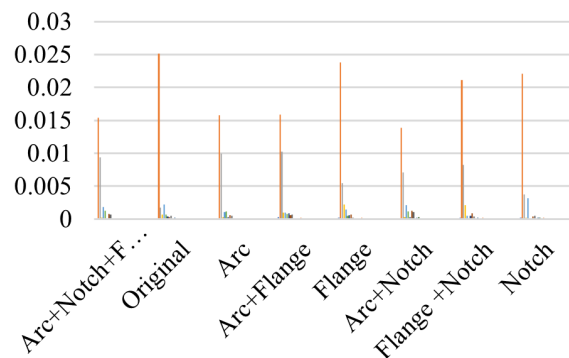


Figure 30. Harmonics of different models.

5.11. Effect of Cogging Torque Reduction Techniques on Torque Ripple

Torque ripple (T_{rip}) is the difference between the maximum torque peak (T_{max}) and minimum torque peak (T_{min}) at the instantaneous torque response and is given as follows:

$$T_{rip} = T_{max} - T_{min} \quad (10)$$

The torque ripples for various rotors are shown in Figure 31. The model with the hybrid notch, flange, and arc had the lowest torque ripples of 0.2926 N-m. The model with the notch and flange cogging torque reduction technique and the model with no cogging torque reduction technique had the largest torque ripples of 3.26% and 2.96%, respectively.

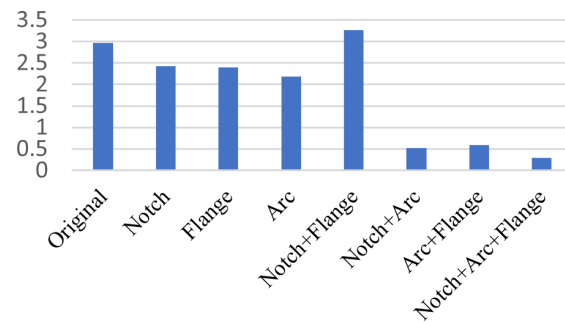


Figure 31. Torque ripples of different models.

5.12. Effect of Cogging Torque Reduction Techniques on Average Torque vs. Current Density

Figure 32 shows the average torque at various armature currents with constant PM field excitation of the rotor with all the study causes discussed above. The highest torque was obtained when using a flange of 2 mm. The average torque increased with increasing armature current density. The maximum increase in average torque of 8 rotor poles with a flange of 2 mm was 15.152%, 5.65 N-m, at a current density of 30 A. All the other techniques caused a decrease in the average torque. The reduction in average torque when applying the arc technique was 46.171%; the notch technique caused the average torque to reduce to 5.25%; the arc and flange technique reduced the average torque to 66.72%; the notch and arc technique reduced the average torque to 63.46%; a reduction of 17.67% in average torque was observed when applying the notch and flange technique; and finally the arc, notch, and flange technique reduced the average torque to 50%, as shown in Figure 32.

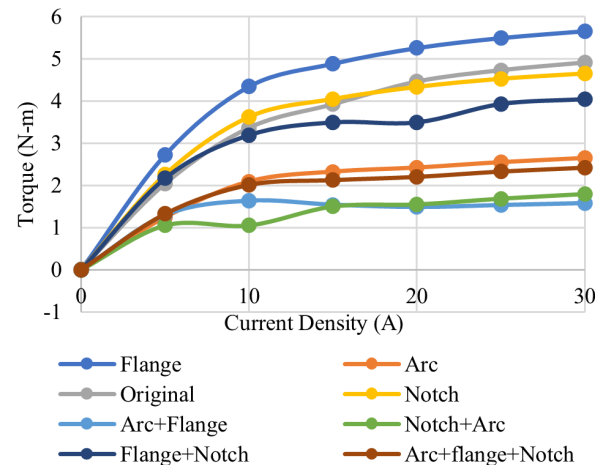


Figure 32. Average torque vs current density of different models.

6. Conclusions

The performance of a modular stator with different rotor pole topologies were presented in this paper. Analysis of no-load flux linkage, cogging torque, average torque, and instantaneous torque on 2D FEA was performed. Initially, different machine topology design procedures were discussed in detail. Furthermore, the load and no-load tests were performed to validate the proposed machine topology. The 8-rotor-pole topologies had the maximum cogging torque; therefore, different cogging torque reduction techniques were applied to reduce the cogging torque. We compared the results of all the cogging torque reduction techniques: torque ripples, no-load flux, no-load back-EMF, average torque, and harmonics of the flux, as shown in Figure 33.

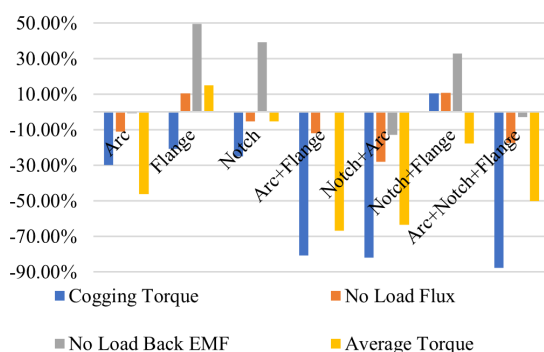


Figure 33. Comparison of cogging torque reduction techniques.

By comparing all the above cogging torque reduction techniques, the cogging torque was reduced by 25%, 29.66%, and 20.66% when the notch, arc, and flange techniques were applied, respectively. Furthermore, by applying hybrid techniques, such as arc flange, arc notch, and arc flange notch, cogging torque was reduced by 8.66%, 82%, and 87.66%, respectively. While 10% cogging torque was observed when applying the notch flange techniques.

Moreover, magnetic flux increased by 10.39% and 10.95% due to the flange and notch flange techniques, respectively. The back-EMF decreased by applying arc, notch, and notch arc flange by 0.846%, 13.83%, and 2.83%, respectively. The average load torque was reduced by 46.17%, 15.28%, 66.72%, 63.46%, 17.45%, and 50% by arc, notch, arc flange, notch arc, notch flange, and arc notch flange, respectively.

Author Contributions: Conceptualization, N.A. and A.P.; methodology, N.A. and S.K.; software, A.P. and A.H.M.; validation, S.A. and K.M.C.; formal analysis, A.P. and K.M.C.; investigation, N.A.; resources, S.A.; data curation, H.A.K.; writing—original draft preparation, N.A. and A.P.; writing—review and editing, S.A. and H.A.K.; visualization, A.H.M.; supervision, N.A.; project administration, S.K. All authors have read and agreed to the published version of the manuscript.

Funding: The authors extend their appreciation to the Deanship of Scientific Research at King Khalid University for funding this work under grant number (RGP.1/133/43).

Institutional Review Board Statement: Not applicable.

Informed Consent Statement: Not applicable.

Data Availability Statement: The data discussed in this research paper are provided on request from the corresponding author. The data are confidential.

Conflicts of Interest: The authors declare no conflict of interest.

Abbreviations

The following abbreviations are used in this manuscript:

PM	Permanent magnet
EMF	Electromotive force
SRM	Switched reluctance machine
FRPMM	Flux reversal permanent magnet machines
FSCW	Fractional slot concentrated winding
FEFRM	Field excited flux reversal machine
HPMFRM	Hybrid permanent magnet flux reversal machine
MSFRPMM	Modular stator flux reversal permanent magnet machine
MS	Modular stator
FEA	Finite element analysis

References

1. Zheng, M.; Zhu, Z.Q.; Cai, S.; Xue, S.S. A novel modular stator hybrid-excited doubly salient synchronous machine with stator slot permanent magnets. *IEEE Trans. Magn.* **2019**, *55*, 1–9. [[CrossRef](#)]
2. Bianchi, N.; Fornasiero, E.; Soong, W. Selection of PM flux linkage for maximum low-speed torque rating in a PM-assisted synchronous reluctance machine. *IEEE Trans. Ind. Appl.* **2015**, *51*, 3600–3608. [[CrossRef](#)]
3. Cao, R.; Mi, C.; Cheng, M. Quantitative comparison of flux-switching permanent-magnet motors with interior permanent magnet motor for EV, HEV, and PHEV applications. *IEEE Trans. Magn.* **2012**, *48*, 2374–2384. [[CrossRef](#)]
4. Ding, W.; Yang, S.; Hu, Y.; Li, S.; Wang, T.; Yin, Z. Design consideration and evaluation of a 12/8 high-torque modular-stator hybrid excitation switched reluctance machine for EV applications. *IEEE Trans. Ind. Electron.* **2017**, *64*, 9221–9232. [[CrossRef](#)]
5. Yang, H.; Zhu, Z.Q.; Liu, Y.; Li, H.Y.; Mipo, J.C. Comparative study of doubly salient machines with/without stator slot permanent magnets. In Proceedings of the 2017 IEEE International Electric Machines and Drives Conference (IEMDC), Miami, FL, USA, 21–24 May 2017; pp. 1–6.
6. Gao, Y.; Li, D.; Qu, R.; Li, J. Design procedure of flux reversal permanent magnet machines. *IEEE Trans. Ind. Appl.* **2017**, *53*, 4232–4241. [[CrossRef](#)]
7. Gao, Y.; Qu, R.; Li, D.; Li, J.; Wu, L. Design of three-phase flux-reversal machines with fractional-slot windings. *IEEE Trans. Ind. Appl.* **2016**, *52*, 2856–2864. [[CrossRef](#)]
8. Wang, C.X.; Boldea, I.; Nasar, S.A. Characterization of three phase flux reversal machine as an automotive generator. *IEEE Trans. Energy Convers.* **2001**, *16*, 74–80. [[CrossRef](#)]
9. More, D.S.; Fernandes, B.G. Analysis of flux-reversal machine based on fictitious electrical gear. *IEEE Trans. Energy Convers.* **2010**, *25*, 940–947. [[CrossRef](#)]
10. Boldea, I.; Zhang, J.; Nasar, S.A. Theoretical characterization of flux reversal machine in low-speed servo drives—the pole-PM configuration. *IEEE Trans. Magn.* **2002**, *38*, 1549–1557. [[CrossRef](#)]
11. Gao, Y.; Qu, R.; Li, D.; Li, J.; Zhou, G. Consequent-pole flux-reversal permanent-magnet machine for electric vehicle propulsion. *IEEE Trans. Appl. Supercond.* **2016**, *26*, 1–5. [[CrossRef](#)]
12. Wu, Z.Z.; Zhu, Z.Q. Partitioned stator flux reversal machine with consequent-pole PM stator. *IEEE Trans. Energy Convers.* **2015**, *30*, 1472–1482. [[CrossRef](#)]
13. Peng, W.; Gyselinck, J. Magnetic-equivalent-circuit modeling of switched reluctance machines with mutual coupling effects. In Proceedings of the 2016 XXII International Conference on Electrical Machines (ICEM), Lausanne, Switzerland, 4–7 September 2016; pp. 426–432.
14. Ding, W.; Hu, Y.; Wang, T.; Yang, S. Comprehensive research of modular E-core stator hybrid-flux switched reluctance motors with segmented and nonsegmented rotors. *IEEE Trans. Energy Convers.* **2016**, *32*, 382–393. [[CrossRef](#)]
15. Anuja, T.A.; Doss, M. Reduction of cogging torque in surface mounted permanent magnet brushless DC motor by adapting rotor magnetic displacement. *Energies* **2021**, *14*, 2861. [[CrossRef](#)]
16. Ravisankar, B.; Senthilnathan, N.; Sethupathi, P. Overview on Various Techniques for Reduction of cogging torque and torque ripples of Permanent Magnet motors of different rotor configurations. In Proceedings of the 2020 International Virtual Conference on Robotics, Automation, Intelligent Systems and Energy (IVC RAISE 2020), Erode, India, 15 December 2020.
17. Zhang, Z.; Zhang, M.; Yin, J.; Wu, J.; Yang, C. An Analytical Method for Calculating the Cogging Torque of a Consequent Pole Hybrid Excitation Synchronous Machine Based on Spatial 3D Field Simplification. *Energies* **2022**, *15*, 878. [[CrossRef](#)]
18. Mengesha, S.; Rajput, S.; Lineykin, S.; Averbukh, M. The Effects of Cogging Torque Reduction in Axial Flux Machines. *Micromachines* **2021**, *12*, 323. [[CrossRef](#)] [[PubMed](#)]
19. Cui, Y.; Zhang, F.; Huang, L.; Chen, Z. Analysis and Verification of a Cogging Torque Reduction Method for Variable Flux Memory Permanent Magnet Machine. *Electronics* **2021**, *10*, 1913. [[CrossRef](#)]
20. Ahmad, N.; Khan, F.; Khan, H.A.; Khan, S.; Khan, F.; Khan, M.A.; Ahmad, I. Effective computational techniques of reducing cogging torque in permanent magnet flux switching machine. *J. Appl. Emerg. Sci.* **2020**, *10*, 19. [[CrossRef](#)]
21. Song, S.; Hu, M.; Xia, Y. Cogging torque optimization and analysis of hybrid stator permanent magnet motor. *Int. J. Appl. Electromagn.* **2021**, *65*, 643–659. [[CrossRef](#)]